

Disconnected entanglement entropy as a marker of edge modes in a periodically driven Kitaev chain

Saikat Mondal^{1,*}, Diptiman Sen^{2,†} and Amit Dutta^{1‡}

¹*Department of Physics, Indian Institute of Technology, Kanpur 208016, India*

²*Centre for High Energy Physics and Department of Physics,
Indian Institute of Science, Bengaluru 560012, India*

We study the disconnected entanglement entropy (DEE) of a Kitaev chain in which the chemical potential is periodically driven in various ways, namely, δ -pulses, square pulse and sinusoidal modulation. In all these cases, the DEE of a sufficiently large system with open boundary conditions turns out to be integer-quantized, with the integer being equal to the number of Majorana edge modes generated by the periodic driving. Thus, the DEE can be considered as a marker for detecting Majorana edge modes in a periodically driven Kitaev chain. Interestingly, we find that the DEE may, in some cases, also detect the anomalous edge modes which can be generated by periodic driving of the nearest-neighbor hopping, even though such modes have no topological significance.

I. INTRODUCTION

There is a recent upsurge in studies of topological phases of matter [1–6]. These phases are robust against weak perturbations due to the existence of a bulk gap, which does not vanish unless the system crosses a gapless quantum critical point (QCP). In addition, a topological phase is characterized by a topological invariant, which remains constant under continuous variations of parameters as long as the system remains in the same phase and becomes ill-defined at QCPs which separate different phases.

In this regard, the Kitaev chain of spinless fermions (a p -wave superconducting system in one dimension) is a paradigmatic model that hosts symmetry protected topologically non-trivial and topologically trivial phases separated by a QCP [7, 8]. The topological properties of a Kitaev chain with periodic boundary conditions is characterized by a topological invariant known as the winding number. The winding number assumes non-zero integer-quantized values in the topologically non-trivial phase and vanishes in the topologically trivial phase. For a system with open boundary conditions, the topologically non-trivial phase of the model is manifested in the existence of zero-energy Majorana modes localized at the edges; on the contrary, the topologically trivial phase does not host Majorana edge modes. The exact solvability of the model has been extensively exploited to understand its equilibrium as well as out-of-equilibrium properties [7–17].

Concerning the non-equilibrium dynamics of closed quantum systems, periodically driven systems have been explored both in the context of thermalization [18–28] and emergent topology [10, 11, 15, 17, 29–50] (for recent review articles, see Refs. [17, 21, 26, 28]). For a periodically driven Kitaev chain, it has been shown that zero-

energy Majorana edge modes can be dynamically generated [11, 15, 17] even though the instantaneous Hamiltonian may remain topologically trivial at all times. In fact, it is the effective Floquet Hamiltonian [51] that determines the non-trivial topology (i.e., the existence of zero-energy Majorana edge modes) of a driven chain. It has been observed that the number of such dynamical edge modes increases as the drive frequency is reduced. Further, a strong (having a sufficiently large amplitude) periodic modulation of the hopping parameter can produce some “anomalous” edge modes with non-zero Floquet quasienergies [15]. However, these anomalous edge modes have no topological significance and topological invariants like the winding number miss them completely.

There have been several attempts to characterize the out-of-equilibrium topology of one-dimensional systems (e.g., the Kitaev chain and the Su-Schrieffer-Heeger chain) using the dynamical winding number calculated from the instantaneous wave function of the system [52–54]. In a periodically driven Kitaev chain, the corresponding winding number [11] is calculated from the Floquet Hamiltonian (for a review, see Ref. [17]). This winding number can correctly predict the number of zero-energy Majorana modes for a Kitaev chain with a periodically kicked (i.e., δ -pulse) chemical potential. However, defining a winding number for a sinusoidal modulation of the chemical potential is more difficult because of the complicated structure of the corresponding Floquet Hamiltonian. Furthermore, the dynamical winding number fails to detect the anomalous edge modes which arise when the hopping parameter is driven strongly [15].

Recently, the notion of a disconnected entanglement entropy (DEE) [55, 56] has been introduced which plays a role similar to a topological invariant in an equilibrium Kitaev chain with an open boundary condition. It is worth noting that unlike the winding number, the DEE is not a bulk topological invariant. Rather, it extracts the entanglement between the Majorana modes localized at the edges. Although the DEE can take any real value by its construction, it turns out to be integer-quantized for a short-ranged Kitaev chain in the topological phase,

* msaikat@iitk.ac.in

† diptiman@iisc.ac.in

‡ dutta@iitk.ac.in

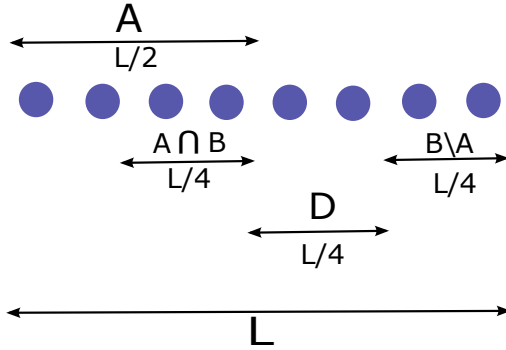


FIG. 1. Partitions of a chain with the disconnected partition $D = \overline{A \cup B}$ and $2L_A = 2L_B = 4L_D = L$. The subsystem B consists of two partitions $A \cap B$ and $B \setminus A$, separated by the disconnected partition D .

where the integer is the total number of edge modes of the system [55–57].

In this paper, we explore the efficacy of the DEE in detecting the dynamically generated edge modes for a periodically driven Kitaev chain. We study the variation of the DEE with the drive frequency for three different types of periodic modulations of the chemical potential, namely, δ -pulses, square pulse and sinusoidal variations. Our study establishes that the DEE correctly predicts the number of edge modes for each of the protocols. We also investigate the applicability of the DEE as a marker of anomalous edge modes appearing due to a periodic modulation of the nearest-neighbor hopping amplitude.

The rest of the paper is organized as follows: the conventional definition of the DEE is introduced in Sec. II. In Sec. III, we briefly recapitulate a short-ranged Kitaev chain of spinless fermions and its topological properties. The behavior of the DEE for a Kitaev chain with periodically modulated chemical potential is explored in Sec. IV. We then briefly compare the DEE with the dynamical winding number derived from the Floquet Hamiltonian of a Kitaev chain with a periodic variation of the chemical potential in Sec. V. In Sec. VI, we study the situation where the nearest-neighbor hopping amplitude is periodically modulated and address the question of whether the DEE can detect the anomalous edge modes. Concluding remarks are presented in Section VII. In Appendix A, we introduce the notion of two equivalent versions of the DEE with different configurations of partitions. In Appendix B, we investigate the behavior of the DEE observed at the stroboscopic instants of time for the protocol discussed in Sec. IV.

II. DISCONNECTED ENTANGLEMENT ENTROPY

In this section, we briefly introduce the notion of disconnected entanglement entropy (DEE) [55, 56]. To this end, we first consider a composite system \mathcal{S} that is in a

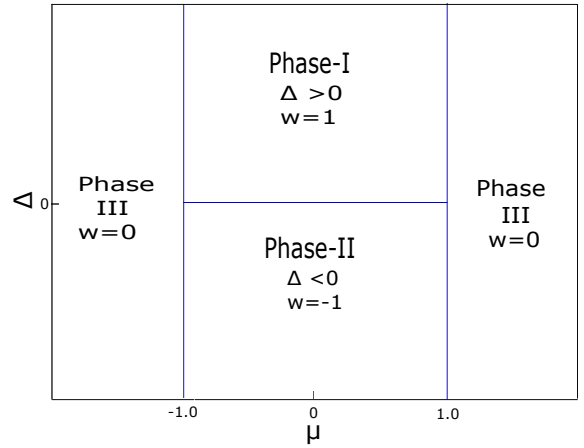


FIG. 2. Phase diagram of a Kitaev chain in the (μ, Δ) plane (we take $\gamma = 1$) showing the winding number w in the different phases. Phases I and II are topological, and the phases marked III are non-topological.

pure state and is described by a density matrix ρ . The reduced density matrix of a subsystem A is obtained by tracing over the degrees of freedom of the rest of the system \bar{A} [58]:

$$\rho_A = \text{Tr}_{\bar{A}}(\rho). \quad (1)$$

The entanglement entropy [59–62] of subsystem A is then defined in terms of the eigenvalues λ_i of the reduced density matrix ρ_A as

$$S_A = -\text{Tr}_A(\rho_A \ln(\rho_A)) = -\sum_i \lambda_i \ln(\lambda_i). \quad (2)$$

As the system \mathcal{S} is in a pure state, it can be shown that $S_A = S_{\bar{A}}$.

We now consider a configuration of the partitions A , B , $A \cap B$ and $A \cup B$ of the system \mathcal{S} , such that the subsystem B consists of two parts $A \cap B$ and $B \setminus A$, separated by the disconnected partition $D = A \cup B$ as shown in Fig. 1. The DEE [55–57] is then defined as

$$S_D = S_A + S_B - S_{A \cup B} - S_{A \cap B}. \quad (3)$$

In Appendix A, we have considered two simple configurations of partitions and shown the equivalence of the DEEs corresponding to these two configurations to the one defined in Eq. (3).

III. KITAEV CHAIN

We recall the Hamiltonian of a Kitaev chain [7–11] with short-ranged interactions given by

$$H = -\gamma \sum_{n=1}^{L-1} (c_n^\dagger c_{n+1} + c_{n+1}^\dagger c_n) - \mu \sum_{n=1}^L (2c_n^\dagger c_n - 1) + \Delta \sum_{n=1}^{L-1} (c_n c_{n+1} + c_{n+1}^\dagger c_n^\dagger), \quad (4)$$

where c_n (c_n^\dagger) is the annihilation (creation) operator for a spinless fermion on the n -th site, γ is the nearest-neighbor hopping parameter, Δ is the strength of the p -wave superconducting pairing, and μ is the on-site chemical potential. The parameters γ , Δ and μ will be taken to be real unless otherwise mentioned. Consequently, the Hamiltonian respects time-reversal symmetry (\mathcal{T}), particle-hole symmetry (\mathcal{P}) and sub-lattice/chiral symmetry (\mathcal{C}).

Assuming periodic boundary conditions, the Hamiltonian H can be written in terms of momentum space fermion creation and annihilation operators as

$$H = \sum_k (c_k^\dagger \ c_{-k}) H_k \begin{pmatrix} c_k \\ c_{-k}^\dagger \end{pmatrix}, \quad (5)$$

where k lies in the range $[-\pi, \pi]$, and the Hamiltonian H_k is given by

$$H_k = (-\gamma \cos k - \mu) \ \sigma_z + \Delta \sin k \ \sigma_y. \quad (6)$$

In the ground state of the Hamiltonian H in Eq. (4), the winding number [11] is defined as

$$w = \frac{1}{2\pi} \int_{-\pi}^{\pi} dk \frac{d\phi_k}{dk}, \quad (7)$$

$$\phi_k = \tan^{-1} \left(\frac{\Delta \sin k}{\gamma \cos k + \mu} \right). \quad (8)$$

Setting the hopping parameter $\gamma = 1$, we show the phase diagram of the ground state of the model in Fig. 2.

1. Topologically non-trivial phase ($-1 < \mu < 1$): This phase consists of phase I ($\Delta > 0$) and phase II ($\Delta < 0$). The winding numbers in phases I and phases II are given by $w = +1$ and $w = -1$, respectively [11]. For a chain with open boundary condition, these topologically non-trivial phases are characterized by the existence of a zero-energy Majorana mode localized at each edge of the chain [11].
2. Topologically trivial phase ($|\mu| > 1$): The winding number is zero ($w = 0$) in this phase. For a chain with open boundary condition, Majorana edge modes do not appear in this phase.

It is noteworthy that in a chain with short-ranged couplings and open boundary conditions, the DEE, calculated in the ground state of static Hamiltonian, is an

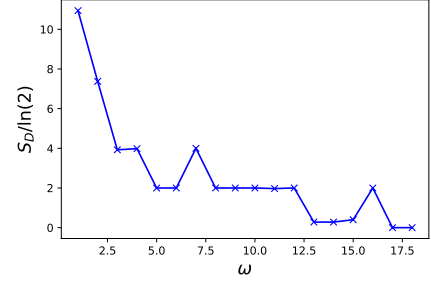


FIG. 3. DEE (S_D) in units of $\ln(2)$ as a function of driving frequency ω for a Kitaev chain in which the chemical potential μ is periodically modulated by δ -pulses (Eq. (10)) with $\mu_0 = 2.5$ and $\mu_1 = 0.2$. We have taken $L = 200$ and $L_D = 50$. The DEE assumes integer-quantized values except at low frequencies. The number of dynamically generated edge Majorana increases as ω decreases.

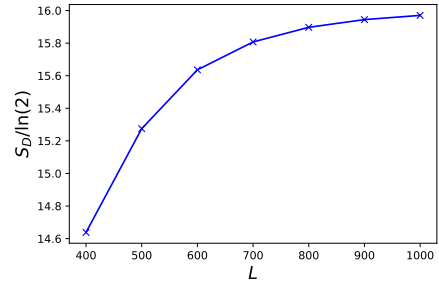


FIG. 4. DEE (S_D) in units of $\ln(2)$ as a function of the length L of a Kitaev chain (with $L_D = L/4$) in which the chemical potential μ is periodically modulated by δ -pulses (Eq. (10)) with $\mu_0 = 2.5$, $\mu_1 = 0.2$, and $\omega = 1$. We observe a saturation to an integer-quantized value as L increases establishing that the discrepancy observed for low ω in Fig. 3 is a finite-size effect.

integer multiple of $\ln(2)$, i.e., $S_D = p \ln(2)$, where p is the total number of modes at the edges of an open system (see Ref. [55–57]). The total number of edge modes is twice the number of modes at each edge. Therefore, the values of the DEE in the topologically non-trivial and trivial phases of a Kitaev chain are $2 \ln(2)$ and zero, respectively, and there is a discontinuous jump in the value of the DEE at the QCP separating the two phases. Thus, the DEE plays a role equivalent to the winding number for an open chain.

IV. DEE FOR A KITAEV CHAIN WITH PERIODICALLY MODULATED CHEMICAL POTENTIAL

We now consider a Kitaev chain with an open boundary condition in which the chemical potential is periodically modulated [11], such that $\mu(t) = \mu(t + T)$, with $T = 2\pi/\omega$ where ω is the driving frequency, so that $H(t)$

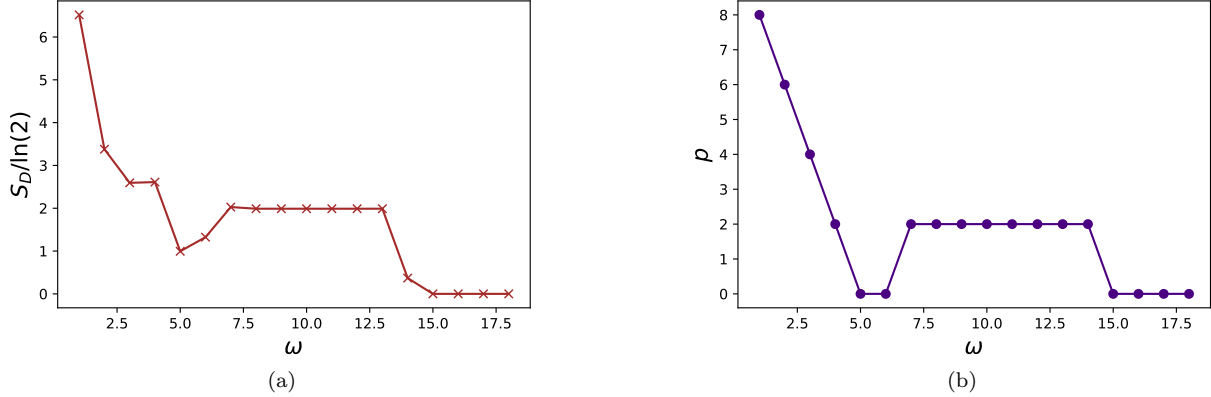


FIG. 5. (a) DEE (S_D) in units of $\ln(2)$ and (b) total number of Majorana edge modes p as functions of ω for a Kitaev chain in which the chemical potential μ is periodically modulated by a square pulse (Eq. (11)) with $\mu_0 = 2.5$ and $\mu_1 = 0.2$. We have taken $L = 200$ and $L_D = 50$.

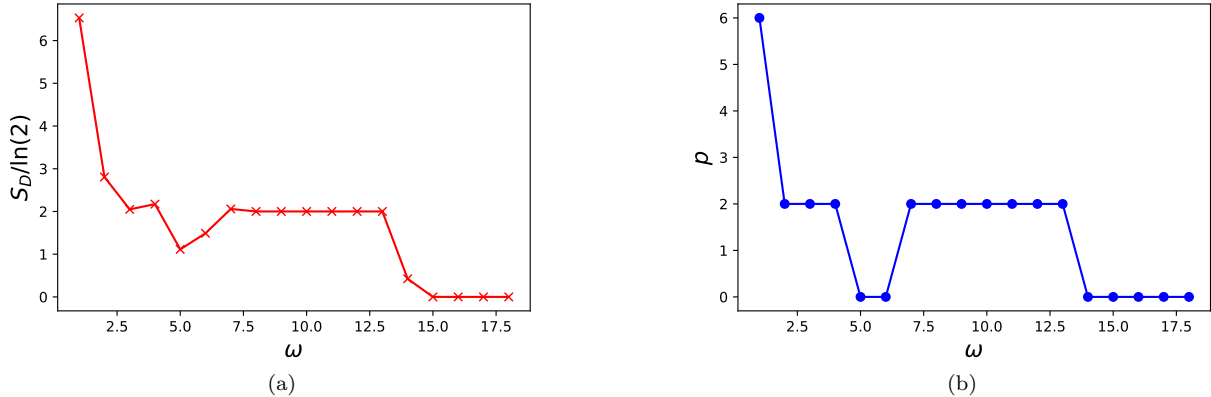


FIG. 6. (a) DEE (S_D) in units of $\ln(2)$ and (b) total number of Majorana edge modes p as functions of ω for a Kitaev chain in which the chemical potential μ is periodically driven with sinusoidal modulation (Eq. (12)) with $\mu_0 = 2.5$, $\mu_1 = 0.3$ and $\phi = 0$. We have taken $L = 200$ and $L_D = 50$.

in Eq. (4) satisfies $H(t) = H(t + T)$. For a time-periodic Hamiltonian $H(t)$, the stroboscopic time-evolution operator (i.e., the Floquet operator) is defined as

$$U_F = \mathbb{T} \exp \left(-i \int_0^T H(t) dt \right) = \exp(-i H_F T), \quad (9)$$

where H_F is the Floquet Hamiltonian and \mathbb{T} denotes time-ordering. (We will set $\hbar = 1$ in this paper).

We recall that due to the unitary nature of the Floquet operator U_F , its eigenvalues are phases. Further, these appear in complex conjugate pairs, $e^{i\theta}$ and $e^{-i\theta}$. If present, Majorana edge modes typically have Floquet eigenvalues $+1$ and -1 corresponding to Floquet quasienergies $\theta = 0$ and $\theta = \pi$, respectively. The number of Majorana edge modes is given by the total number of Floquet eigenvalues $+1$ and -1 . We now explore the variation of the DEE in the ground state of the effective

Floquet Hamiltonian as a function of the drive frequency ω for three different driving protocols.

We will also discuss the behavior of the DEE observed at the stroboscopic instants of time in Appendix B. In this case, we obtain a critical drive frequency ω_c , such that for $\omega > \omega_c$, the DEE becomes independent of ω for a particular stroboscopic instant.

A. Periodic δ -pulse modulation of μ

We now consider the protocol in which the chemical potential μ is periodically modulated by the application of δ -pulses such that [11, 17]

$$\mu(t) = \mu_0 + \mu_1 \sum_{n=-\infty}^{\infty} \delta(t - nT), \quad (10)$$

where $T = 2\pi/\omega$. In this driving protocol, the DEE, calculated in the ground state of the Floquet Hamiltonian, is equal to integer multiples of $\ln(2)$, as can be seen from Fig. 3. It is also interesting to note that the DEE generally increases as the drive-frequency (ω) decreases. Further, we have verified that the value of $S_D/\ln(2)$ is equal to the number of Majorana modes generated by the same periodic driving of the Kitaev chain as studied in Ref. [11].

However, at low drive frequencies, the DEE is not integer-quantized and the value of $S_D/\ln(2)$ differs significantly from the number of Majorana end modes. This is however a finite-size effect, as shown in Fig. 4, which demonstrates that the DEE does saturate to an integer-quantized value for large system size L . The reason for the finite-size effect is that more and more of the Majorana end modes which appear at low drive frequencies have large decay lengths. When the decay length is comparable to the size $L/4$ of the disconnected region D , the contribution of such end modes to the DEE deviates from integer multiples of $\ln(2)$.

B. Periodic square pulse modulation of μ

Let the chemical potential μ be periodically modulated by square pulses of the form

$$\mu(t) = \begin{cases} \mu_0 + \mu_1, & \text{for } 0 < t < \frac{T}{2}, \\ \mu_0 - \mu_1, & \text{for } \frac{T}{2} < t < T, \end{cases} \quad (11)$$

where $T = 2\pi/\omega$. From Fig. 5, we observe that the value of $S_D/\ln(2)$ is integer-quantized and is equal to total number p of Majorana edge modes generated by the same square pulse, unless the drive frequency is sufficiently small. We reiterate that the discrepancy in the value of $S_D/\ln(2)$ at low drive frequencies occurs due to the finiteness of the system size L .

C. Sinusoidal modulation of μ

Finally, for a sinusoidal variation of μ of the form

$$\mu(t) = \mu_0 + \mu_1 \sin(\omega t + \phi), \quad (12)$$

we obtain similar results for the DEE as shown in Fig. 6.

V. COMPARISON OF THE DEE WITH THE DYNAMICAL WINDING NUMBER FOR PERIODICALLY DRIVEN KITAEV CHAIN

In this section, we compare the results inferred from the behavior of the DEE with the dynamical winding number for driving protocols discussed in Sec. IV.

For a periodically driven Kitaev chain with periodic boundary conditions, the winding number may be calculated from the stroboscopic time-evolution operator (i.e.,

Floquet operator)

$$U_F(k) = \mathbb{T} \exp \left(-i \int_0^T H_k(t) dt \right) = \exp(-i h_k^F T), \quad (13)$$

for momentum $k \in [-\pi, \pi]$, where h_k^F and $H_k(t)$ are, respectively, the Floquet Hamiltonian and the instantaneous Hamiltonian for the mode with momentum k . Referring to Eq. (6), for a generic time-dependent chemical potential, we get

$$H_k(t) = (-\gamma \cos k - \mu(t)) \sigma_z + \Delta \sin k \sigma_y. \quad (14)$$

For a periodic driving, we can present the general form of the Floquet Hamiltonian h_k^F [11, 15] as

$$h_k^F = d_0(k) \mathbb{1} + d_x(k) \sigma_x + d_y(k) \sigma_y + d_z(k) \sigma_z, \quad (15)$$

where $\sigma_x, \sigma_y, \sigma_z$ are Pauli matrices, and $\mathbb{1}$ is the 2×2 identity matrix. The coefficients d_0, d_x, d_y and d_z assume different forms for different driving protocols.

If the chemical potential is periodically modulated with δ -pulses (Eq. (10)), the symmetrized Floquet operator $U_F(k)$ is given by

$$U_F(k) = e^{i \frac{\mu_1}{2} \sigma_z} e^{-iT[(-\gamma \cos k - \mu_0) \sigma_z + \Delta \sin k \sigma_y]} e^{i \frac{\mu_1}{2} \sigma_z}. \quad (16)$$

We can analytically show that $d_0(k) = 0$ (since the three matrices in Eq. (16) are all $SU(2)$ matrices) and $d_x(k) = 0$ (since $\sigma_x U_F(k) \sigma_x = [U_F(k)]^{-1}$ for all $k \in [-\pi, \pi]$; we can see in Fig. 7(a) that this is true). We then arrive at a simplified form of the Floquet Hamiltonian h_k^F

$$h_k^F = d_y(k) \sigma_y + d_z(k) \sigma_z. \quad (17)$$

This particular form of h_k^F enables us to define a dynamical winding number [11] in the following way: $d_z(k)$ is plotted as a function of $d_y(k)$ (see Figs. 7(b), 7(c) and 7(d)) and the number of times the curve winds around the origin (located at $d_y = 0, d_z = 0$) is counted. This gives the value of the winding number, which turns out to be equal to the number of zero-energy Majorana modes at each end of an open chain. Thus, the winding number is able to characterize the topology of the Kitaev chain periodically driven with a δ -pulse. On the other hand, the DEE, which can assume any real value, turns out to be an integer multiple of $\ln(2)$ (see Fig. 3). The equivalence of the DEE with the winding number in detecting the Majorana edge modes for the periodic modulation with a δ -pulse is thus established.

For the periodic driving of the chemical potential with a square pulse (for the protocol defined in Eq. (11)) or a sinusoidal modulation (Eq. (12)), we again have $d_0 = 0$ but d_x, d_y, d_z are generally non-zero for $k \in [-\pi, \pi]$, as can be seen from Figs. 8(a) and 8(b). Since the three coefficients d_x, d_y and d_z are non-zero (and hence the vector \vec{d} is not confined to a plane), the winding number cannot be defined for the present choice of these two driving protocols. However, as is evident from Fig. 5(a) and

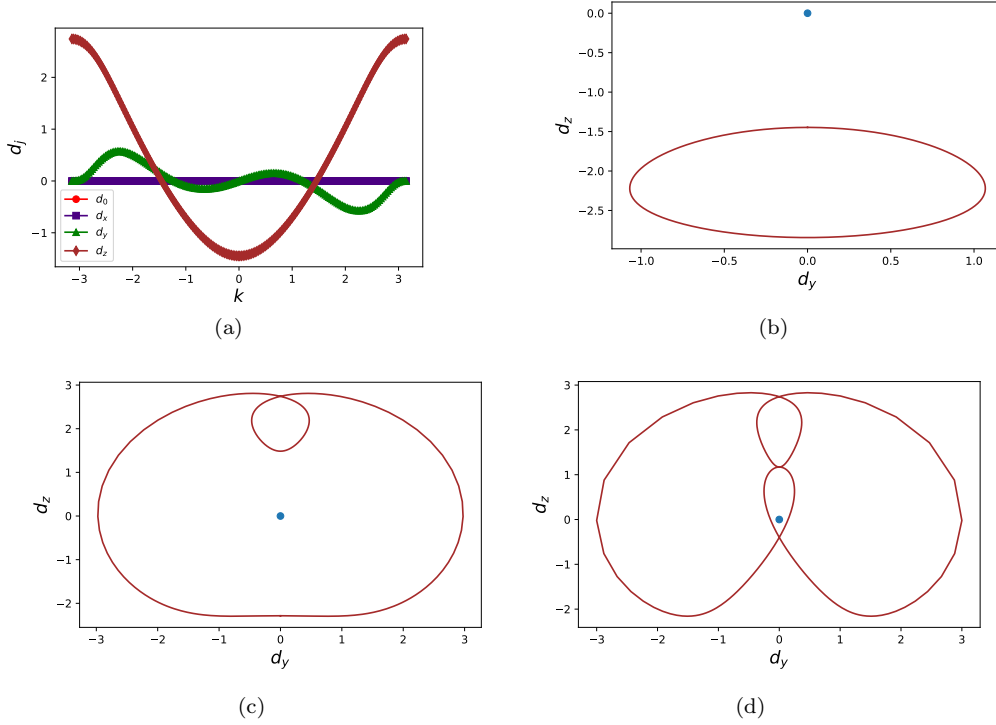


FIG. 7. (a) d_0 , d_x , d_y and d_z as functions of k for periodic driving of the chemical potential with a δ -pulse having $c_0 = 2.5$, $c_1 = 0.2$, and $\omega = 6.0$. We find that $d_0 = 0$ and $d_x = 0$ for all values of k . (b) d_z as a function of d_y for $\omega = 18.0$. The winding number is zero. (c) d_z as a function of d_y for $\omega = 10.0$. The winding number is 1. (d) d_z as a function of d_y for $\omega = 4.0$. The winding number is 2.

Fig. 6(a), the DEE can correctly characterize the emergent topology of the chain for these two protocols. Thus, the DEE successfully detects the dynamically generated zero-energy edge Majorana modes even when a winding number cannot be derived from the associated Floquet Hamiltonian.

VI. DETECTION OF THE ANOMALOUS EDGE MODES IN A KITAEV CHAIN WITH PERIODICALLY MODULATED HOPPING PARAMETER THROUGH DEE

We now consider the periodic driving of the hopping parameter γ , which may be complex in general, so that the Hamiltonian in (4) is modified to

$$H(t) = - \sum_{n=1}^{L-1} (\gamma(t) c_n^\dagger c_{n+1} + \gamma^*(t) c_{n+1}^\dagger c_n) - \mu \sum_{n=1}^L (2c_n^\dagger c_n - 1) + \sum_{n=1}^{L-1} \Delta (c_n c_{n+1} + c_{n+1}^\dagger c_n^\dagger). \quad (18)$$

It has been established that for this type of driving protocol, modes localized at the edges with Floquet eigenvalues away from ± 1 (referred to as anomalous modes) can

dynamically emerge [15]. We address here the question of whether the DEE can detect these anomalous modes.

A. Periodic driving of the amplitude of the hopping parameter

We consider the following form of the hopping parameter,

$$\gamma(t) = \gamma_0 (1 + a \cos(\omega t)), \quad (19)$$

where $\omega = 2\pi/T$, and a determines the strength of the modulation of the hopping amplitude. Since the hopping parameter is chosen to be real, the time-reversal symmetry of the Hamiltonian $H(t)$ is preserved.

To see if there are emergent anomalous modes, we plot the Floquet quasienergies θ as a function of ω for $a = 1$ in Fig. 9(a). Evidently, for $1.5 < \omega < 2.0$, the extreme values (near the top and bottom) of the Floquet quasienergies are separated by finite gaps from the other quasienergies. The modes with these isolated values of Floquet quasienergies are known as anomalous modes [15] since the corresponding eigenvalues of the Floquet operator differ from ± 1 .

In Fig. 9(b), the variation of the inverse participation ratio (IPR) is plotted against the real part of the corresponding eigenvalues of the Floquet operator for $\omega = 1.7$.

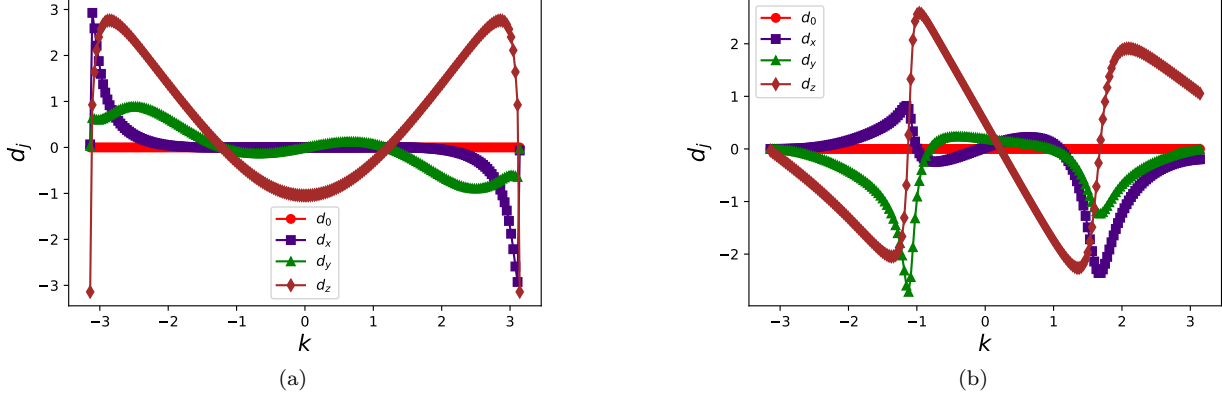


FIG. 8. d_0 , d_x , d_y and d_z as functions of k for (a) periodic driving of chemical potential with square pulses having $c_0 = 2.5$, $c_1 = 0.2$ and $\omega = 6.0$, (b) periodic driving of chemical potential with a sinusoidal modulation having $c_0 = 2.5$, $c_1 = 0.3$ and $\omega = 6.0$. In both cases, we find that $d_0 = 0$ for all values of k .

(For a normalized wave function $\psi_j(n)$, where j labels the wave function and n denotes the site index, the IPR is defined as $\sum_n |\psi_j(n)|^4$. It is known that as the system size L is taken to infinity, the IPRs of modes which are extended in the bulk go to zero while the IPRs of modes localized at the ends remain finite. Hence a plot of the IPR versus j provides an easy way to identify the edge modes). From this figure, it can clearly be seen that the anomalous modes (having the minimum real part of the Floquet eigenvalue) have relatively large IPRs, compared to the other modes having non-zero Floquet quasienergies. We note here that the IPRs of the anomalous modes are almost comparable to that of the zero-energy Majorana modes (with Floquet eigenvalue +1). Fig. 9(c) further confirms that these anomalous modes, despite having non-zero Floquet quasienergies, are localized at the edges of the chain [15].

In Fig. 9(d), the DEE S_D is plotted as a function of the drive frequency ω to find the contribution of these anomalous modes to the DEE. As is evident from Fig. 9(d), the non-zero and integer-quantized contribution of the anomalous modes to the DEE enables us to detect these edge modes. However, comparing the value of the DEE with the IPR for different values of ω (see Fig. 9(e)), we observe that the DEE matches exactly with the total number of edge modes (the zero-energy Majorana modes as well as the anomalous modes) for some frequencies ($\omega \sim 1.8$), but does not match with the same for some other frequencies ($\omega \sim 1.5$). The reason for this discrepancy is not clear.

B. Periodic driving of the phase of the complex hopping parameter

Now we consider the hopping parameter to be complex [15], with the form

$$\gamma(t) = \gamma_0 \exp [ia \cos(\omega t)], \quad (20)$$

where $\omega = 2\pi/T$, and the a determines the strength of the modulation of the phase of the hopping parameter. The complex hopping parameter in Eq. (20) explicitly breaks the time-reversal symmetry of the Hamiltonian $H(t)$ [12, 15].

Similar to the driving protocol discussed in Sec. VI A, by inspecting Figs. 10(a), 10(b) and 10(c), we establish the existence of anomalous edge modes for the protocol in Eq. (20) in the frequency range $1.4 < \omega < 1.7$. To investigate whether these anomalous edge modes are manifested in the DEE, S_D is plotted as a function ω in Fig. 10(d). As we observe in that figure, the DEE has an integer-quantized contribution from these anomalous modes. However, when we compare the value of the DEE with the IPRs for different values of ω (see Fig. 10(e)), we find that the DEE does not match the total number of the edge modes (both zero-energy modes and anomalous modes) for almost all the frequencies. Nevertheless, we observe another interesting feature for $\omega \sim 1.55$: the IPRs of the two zero-energy modes (with $j = 2L - 2$ and $j = 2L - 1$ in Fig. 10(e)) are much smaller than that for the anomalous edge modes and the value of the DEE is exactly $4 \ln(2)$. This implies that only the anomalous modes contribute to the DEE at this frequency. The much smaller IPRs imply that the decay lengths of the zero-modes are comparatively larger, and thus the DEE cannot detect these two zero-energy modes.

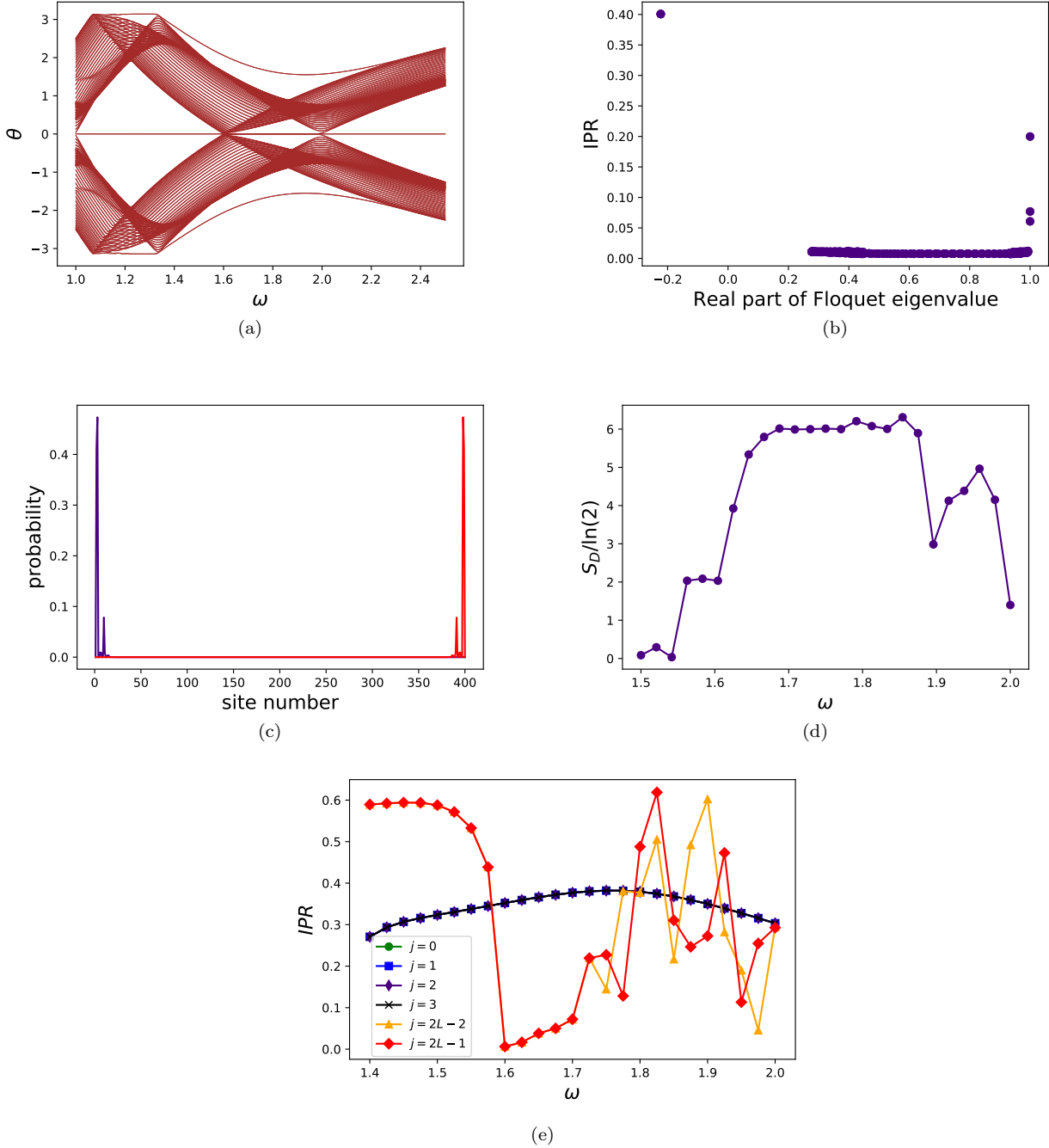


FIG. 9. (a) Floquet quasienergies θ as a function of the drive frequency ω (the two isolated lines seen near the top and bottom in the frequency range of about $[1.4, 2.2]$ correspond to anomalous end modes), (b) inverse participation ratio (IPR) as a function of the real part of the Floquet eigenvalue at $\omega = 1.7$ and for $L = 200$, (c) probability as a function of the site number for two anomalous modes both with Floquet eigenvalue $-0.2229 + 0.9785i$ at $\omega = 1.7$, (d) DEE (S_D) in units of $\ln(2)$ as a function of ω for $L = 400$ and $L_D = 100$, (e) the highest six IPRs of the modes (these include both zero-energy modes and anomalous modes) as a function of ω . The index j denotes the ascending order of the real part of the eigenvalues of the Floquet operator. For all the plots, the amplitude of the hopping parameter is periodically modulated (see Eq. (19)) with $a = 1.0$. We have taken $\mu = 0$, $\Delta = 0.8$ and $\gamma_0 = 1.0$.

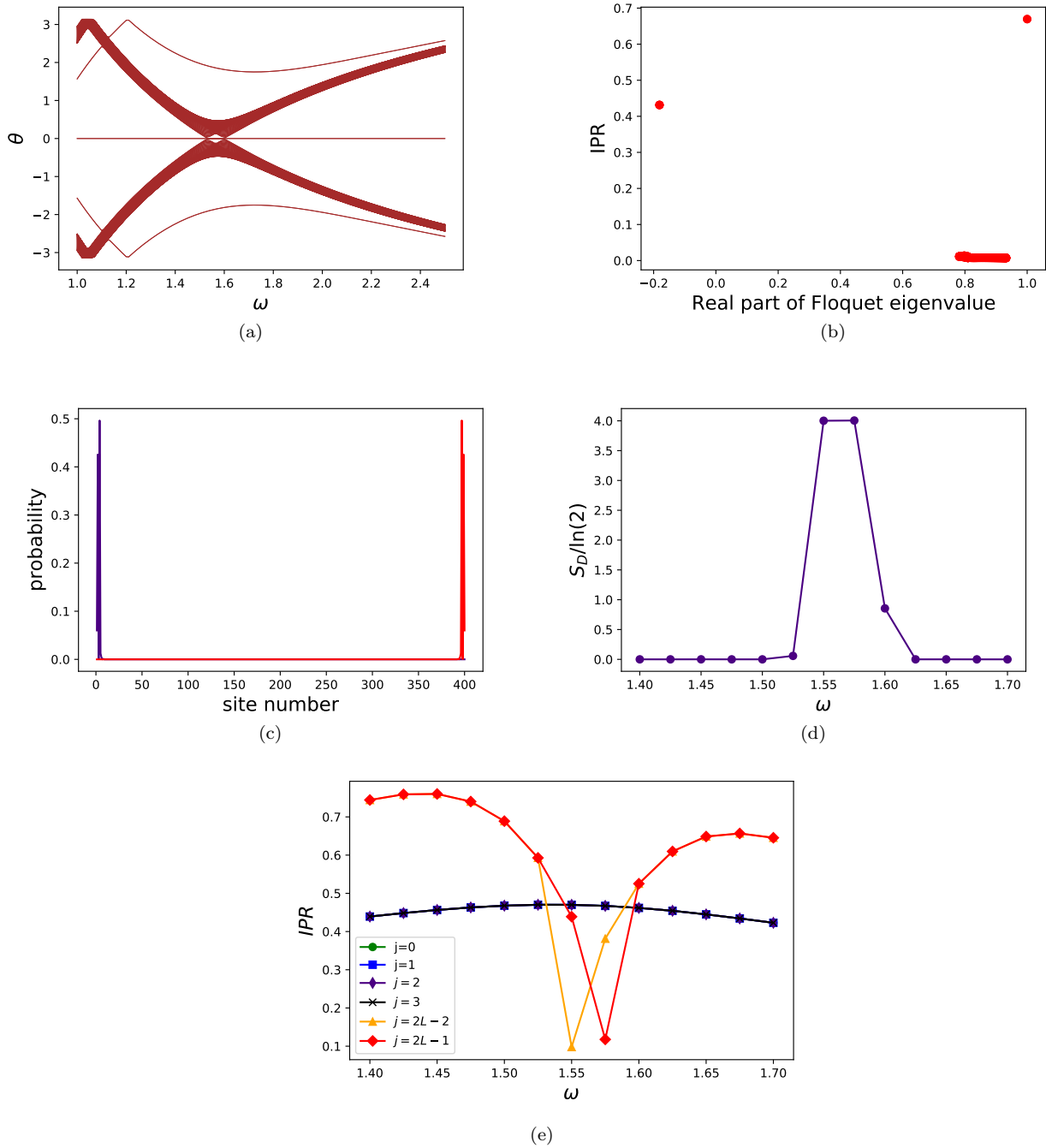


FIG. 10. (a) Floquet quasienergies θ as a function of the drive frequency ω (the two isolated lines seen near the top and bottom for almost the entire range of ω correspond to anomalous end modes), (b) inverse participation ratio (IPR) as a function of the real part of the Floquet eigenvalue at $\omega = 1.7$ and for $L = 200$, (c) probability as a function of site number for two anomalous modes both with Floquet eigenvalue $-0.1813 + 0.9834i$ at $\omega = 1.7$, (d) DEE (S_D) in units of $\ln(2)$ as a function of ω for $L = 200$ and $L_D = 50$, (e) the highest six IPRs of the modes (which include both zero-energy modes and anomalous modes) as a function of ω . The index j denotes the ascending order of the real part of the eigenvalues of the Floquet operator. For all the plots, the phase of the hopping parameter is periodically modulated (Eq. (20)) with $a = 1.0$. Other parameters chosen for the plots are: $\mu = 0$, $\Delta = 0.8$, and $\gamma_0 = 1.0$.

VII. CONCLUSIONS

In this paper, we have shown that for three different driving protocols of the chemical potential, the DEE, calculated in the ground state of the Floquet Hamiltonian, is integer-quantized, with the integer being equal to the total number of dynamically generated Floquet Majorana edge modes. Thus, it can be inferred that similar to the static situation, the DEE can act as a marker of Majorana edge modes even for a periodically driven Kitaev chain. However, at a sufficiently low frequency, there is an apparent discrepancy and the value of $S_D/\ln(2)$ differs significantly from the number of Majorana end modes. This is an artefact of the finite size of the system, and we have established that the DEE saturates to an integer-quantized value at large system size L , even at low drive frequencies (ω of the order of the hopping amplitude γ). What is important is that the DEE correctly counts the number of edge Majorana modes even for driving protocols (with square pulse and sinusoidal variations) for which we cannot easily derive a dynamical winding number from the Floquet Hamiltonian.

If either the phase or the amplitude of the nearest-neighbor hopping in the Kitaev chain is periodically modulated, then ‘anomalous’ edge modes (with Floquet quasienergies not equal to zero or π) can be dynamically generated. Although these anomalous edge modes do not have a topological origin and are not associated with a winding number, we find that the DEE is able to detect the existence of the anomalous edge modes for certain ranges of driving frequencies.

ACKNOWLEDGMENTS

S.M. acknowledges financial support from PMRF fellowship, MHRD, India. D.S. thanks SERB, India for funding through Project No. JBR/2020/000043. A.D. acknowledges support from SPARC program, MHRD, India and SERB, DST, New Delhi, India. We acknowledge Souvik Bandyopadhyay and Sourav Bhattacharjee for comments.

Appendix A: Equivalence of two different configurations of the partitions

We consider the configurations of the partitions in Figs. 11(a) and 11(b) denoted as P_1 and P_2 , respectively. We start with the configuration P_1 . The DEE for P_1 is given by

$$(S_D)_{P_1} = S_A + S_B - S_{A \cup B} - S_{A \cap B}, \quad (A1)$$

with the partition $D = \overline{A \cup B}$. In P_1 , we have $A \cap B = 0$ since there is no region common to A and B . Then, the DEE in Eq. (A1) reduces to

$$(S_D)_{P_1} = S_A + S_B - S_{A \cup B}. \quad (A2)$$

We take $A = \overline{X}$ and $B = \overline{Y}$. Then Eq. (A2) can be recast as

$$\begin{aligned} (S_D)_{P_1} &= S_{\overline{X}} + S_{\overline{Y}} - S_{\overline{X \cup Y}}, \\ \implies (S_D)_{P_1} &= S_{\overline{X}} + S_{\overline{Y}} - S_{\overline{X \cap Y}}, \end{aligned} \quad (A3)$$

where we have used $\overline{X \cup Y} = \overline{X \cap Y}$. Similarly, the partition D can be rewritten as, $D = \overline{A \cup B} = \overline{\overline{X} \cup \overline{Y}} = X \cap Y$. Since $A \cap B = 0$, we have $\overline{X \cap Y} = 0 = \overline{X \cup Y}$, which implies that $X \cup Y$ is the entire system.

We now consider the configuration P_2 in which X has $3L/4$ sites from the left, Y has $3L/4$ sites from the right, and $X \cap Y$ has $L/2$ sites in the middle. The DEE can be written as

$$(S_D)_{P_2} = S_X + S_Y - S_{X \cap Y}, \quad (A4)$$

as $S_{X \cup Y} = 0$ (since $X \cup Y$ is the entire system and it is in a pure state). Then, substituting $S_X = S_{\overline{X}}$, $S_Y = S_{\overline{Y}}$ and $S_{X \cap Y} = S_{\overline{X \cap Y}}$ in Eq. (A4), we obtain the equation

$$(S_D)_{P_2} = S_{\overline{X}} + S_{\overline{Y}} - S_{\overline{X \cap Y}}. \quad (A5)$$

From Eqs. (A3) and (A5), it can be clearly seen that $(S_D)_{P_1} = (S_D)_{P_2}$ and $D = \overline{A \cup B} = X \cap Y$. In fact, the regions \overline{X} and \overline{Y} are ‘disconnected’ by this region $X \cap Y$ in P_2 . Thus, the region $X \cap Y$ in P_2 acts similarly to the region D in P_1 . Therefore, the configuration P_2 can be thought as the ‘dual configuration’ of P_1 .

Appendix B: Behavior of DEE observed at stroboscopic instants of time

We consider a Kitaev chain with the chemical potential $\mu = \mu_0$ at $t = 0$. The chain is periodically driven with the Hamiltonian $H(t)$ in Eq. (4) starting from $t = 0$ following the protocol given in Eq. (10). If the system is initially prepared in an eigenstate $|\psi_0\rangle$ of the Hamiltonian H_0 , then at any stroboscopic instant $t = NT$, the state of the system is given by

$$|\psi(NT)\rangle = U_F^N |\psi_0\rangle, \quad (B1)$$

where $U_F = \mathbb{T} \exp\left(-i \int_0^T H(t') dt'\right) = \exp(-iH_F T)$ is the Floquet operator, and H_F is the Floquet Hamiltonian. We define an effective Hamiltonian [56, 57]

$$H_{\text{eff}}(NT) = U_F^N H_0 (U_F^N)^\dagger, \quad (B2)$$

such that $|\psi_0\rangle$ and $|\psi(NT)\rangle$ are the eigenstates of the Hamiltonians H_0 and $H_{\text{eff}}(NT)$ respectively, with the same energy eigenvalue. Using the Baker-Campbell-Hausdorff (BCH) formula, Eq. (B2) can be recast as

$$H_{\text{eff}}(NT) = H_0 + \sum_{r=1}^{\infty} \frac{(-iNT)^r}{r!} K_r(H_F, H_0), \quad (B3)$$

where $K_r(H_F, H_0) = [H_F, [H_F, [H_F, [H_F, [H_F, H_0] \dots]]]]$, with the Hamiltonian H_F appearing r -times (see Ref. [56, 57]).

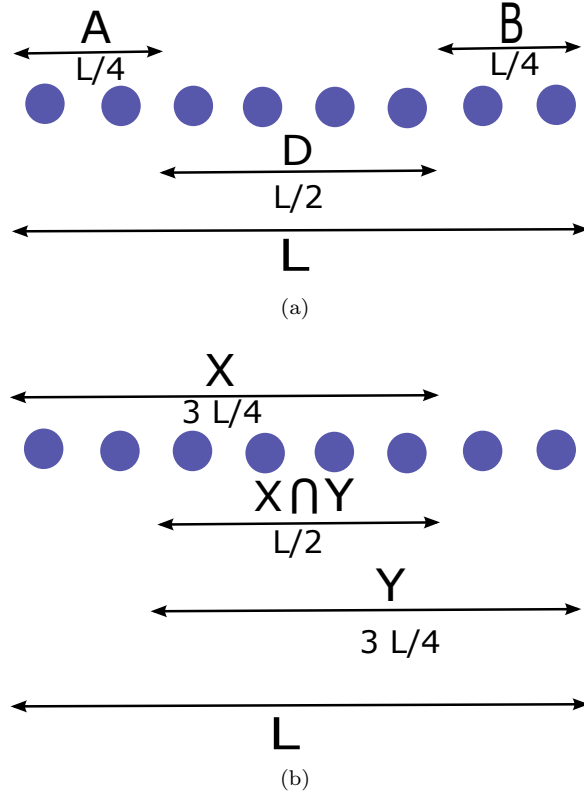


FIG. 11. (a) Configuration P_1 with partition lengths $L_A = L/4$, $L_B = L/4$, $L_D = L_{\overline{A \cup B}} = L/2$, and $A \cap B = 0$, and (b) configuration P_2 with partition lengths $L_X = 3L/4$, $L_Y = 3L/4$, and $L_{X \cap Y} = L/2$.

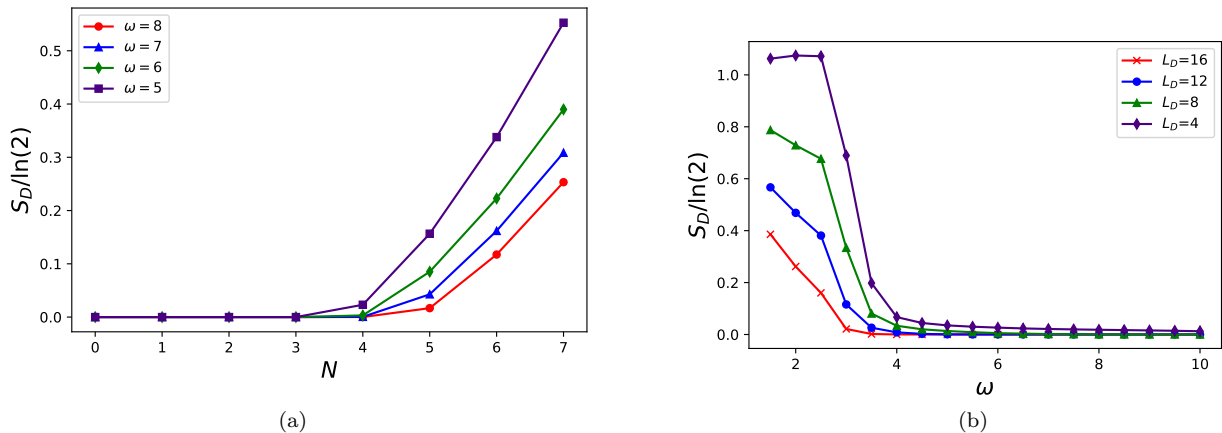


FIG. 12. (a) DEE (S_D) as a function of the stroboscopic instant N for different drive frequencies ω . We have taken $L = 40$ and $L_D = 10$. (b) DEE, calculated at the stroboscopic instant $N = 10$, as a function of ω for a Kitaev chain with $L = 40$ for various lengths(L_D) of the disconnected partition. The critical drive frequency ω_c decreases as L_D increases. In both plots, the chemical potential μ is periodically modulated by δ -pulses (Eq. (10)) with $\mu_0 = 2.5$ and $\mu_1 = 0.2$.

Following the explicit calculation presented in Ref. [57], it can be shown that the effective maximum range r_{\max} of the couplings in the effective Hamiltonian H_{eff} increases with the stroboscopic time $t = NT$.

Now, if the maximum range of interaction of H_{eff} spans the complete disconnected partition D or greater (see

Fig. 1), bulk states start becoming entangled over regions exceeding the disconnected partition size. This starts introducing bulk contributions to the DEE just as in long-ranged interacting Hamiltonians [57], which in turn breaks the temporal invariance of the DEE. Hence, a finite disconnected partition size gives rise to a criti-

cal time scale in a short-ranged system until which the DEE remains temporally invariant. We therefore define a critical time t_c , such that $r_{\max}(t_c) \sim L_D$. Assuming a finite velocity of the increasing range of H_{eff} , we then infer that the critical time t_c grows linearly with the system size L_D . Assuming $t_c = N_c T$ and $T = 2\pi/\omega$, we can also find the critical stroboscopic instant, $N_c \sim \omega$, below which the DEE remains invariant with the varia-

tion of N for that particular ω and above which the DEE starts varying with time. On the contrary, if we vary ω keeping N fixed, then it is possible to find a critical drive frequency, $\omega_c \sim 2\pi N/t_c \sim 2\pi N/L_D$, such that for drive frequencies above that the DEE remains constant with the variation of ω for that particular fixed N . The existence of N_c and ω_c is evident from Figs. 12(a) and 12(b), respectively.

[1] M. Z. Hasan and C. L. Kane, Colloquium: Topological insulators, *Rev. Mod. Phys.* **82**, 3045 (2010).

[2] X.-L. Qi and S.-C. Zhang, Topological insulators and superconductors, *Rev. Mod. Phys.* **83**, 1057 (2011).

[3] L. Fidkowski and A. Kitaev, Topological phases of fermions in one dimension, *Phys. Rev. B* **83**, 075103 (2011).

[4] X. Chen, Z.-C. Gu, Z.-X. Liu, and X.-G. Wen, Symmetry protected topological orders and the group cohomology of their symmetry group, *Phys. Rev. B* **87**, 155114 (2013).

[5] T. Senthil, Symmetry-protected topological phases of quantum matter, *Annual Review of Condensed Matter Physics* **6**, 299 (2015), <https://doi.org/10.1146/annurev-conmatphys-031214-014740>.

[6] C.-K. Chiu, J. C. Y. Teo, A. P. Schnyder, and S. Ryu, Classification of topological quantum matter with symmetries, *Rev. Mod. Phys.* **88**, 035005 (2016).

[7] A. Y. Kitaev, Unpaired majorana fermions in quantum wires, *Physics-Uspekhi* **44**, 131 (2001).

[8] A. Kitaev and C. Laumann, Topological phases and quantum computation 10.48550/arxiv.0904.2771 (2009).

[9] W. DeGottardi, D. Sen, and S. Vishveshwara, Topological phases, majorana modes and quench dynamics in a spin ladder system, *New Journal of Physics* **13**, 065028 (2011).

[10] W. DeGottardi, D. Sen, and S. Vishveshwara, Majorana fermions in superconducting 1d systems having periodic, quasiperiodic, and disordered potentials, *Phys. Rev. Lett.* **110**, 146404 (2013).

[11] M. Thakurathi, A. A. Patel, D. Sen, and A. Dutta, Floquet generation of majorana end modes and topological invariants, *Phys. Rev. B* **88**, 155133 (2013).

[12] W. DeGottardi, M. Thakurathi, S. Vishveshwara, and D. Sen, Majorana fermions in superconducting wires: Effects of long-range hopping, broken time-reversal symmetry, and potential landscapes, *Phys. Rev. B* **88**, 165111 (2013).

[13] A. Rajak and A. Dutta, Survival probability of an edge majorana in a one-dimensional p -wave superconducting chain under sudden quenching of parameters, *Phys. Rev. E* **89**, 042125 (2014).

[14] A. Dutta, G. Aeppli, B. K. Chakrabarti, U. Divakaran, T. F. Rosenbaum, and D. Sen, *Quantum Phase Transitions in Transverse Field Spin Models: From Statistical Physics to Quantum Information* (Cambridge University Press, 2015).

[15] S. Saha, S. N. Sivarajan, and D. Sen, Generating end modes in a superconducting wire by periodic driving of the hopping, *Phys. Rev. B* **95**, 174306 (2017).

[16] S. Bandyopadhyay, S. Bhattacharjee, and A. Dutta, Dynamical generation of majorana edge correlations in a ramped kitaev chain coupled to nonthermal dissipative channels, *Phys. Rev. B* **101**, 104307 (2020).

[17] S. Bandyopadhyay, S. Bhattacharjee, and D. Sen, Driven quantum many-body systems and out-of-equilibrium topology, *Journal of Physics: Condensed Matter* **33**, 393001 (2021).

[18] A. Russomanno, A. Silva, and G. E. Santoro, Periodic steady regime and interference in a periodically driven quantum system, *Phys. Rev. Lett.* **109**, 257201 (2012).

[19] M. Tomka, A. Polkovnikov, and V. Gritsev, Geometric phase contribution to quantum nonequilibrium many-body dynamics, *Phys. Rev. Lett.* **108**, 080404 (2012).

[20] T. Nag, S. Roy, A. Dutta, and D. Sen, Dynamical localization in a chain of hard core bosons under periodic driving, *Phys. Rev. B* **89**, 165425 (2014).

[21] M. Bukov, L. D'Alessio, and A. Polkovnikov, Universal high-frequency behavior of periodically driven systems: from dynamical stabilization to floquet engineering, *Advances in Physics* **64**, 139 (2015), <https://doi.org/10.1080/00018732.2015.1055918>.

[22] S. Dasgupta, U. Bhattacharya, and A. Dutta, Phase transition in the periodically pulsed dicke model, *Phys. Rev. E* **91**, 052129 (2015).

[23] T. Nag, D. Sen, and A. Dutta, Maximum group velocity in a one-dimensional model with a sinusoidally varying staggered potential, *Phys. Rev. A* **91**, 063607 (2015).

[24] A. Sen, S. Nandy, and K. Sengupta, Entanglement generation in periodically driven integrable systems: Dynamical phase transitions and steady state, *Phys. Rev. B* **94**, 214301 (2016).

[25] B. Mukherjee, A. Sen, D. Sen, and K. Sengupta, Signatures and conditions for phase band crossings in periodically driven integrable systems, *Phys. Rev. B* **94**, 155122 (2016).

[26] A. Eckardt, Colloquium: Atomic quantum gases in periodically driven optical lattices, *Rev. Mod. Phys.* **89**, 011004 (2017).

[27] T. Oka and S. Kitamura, Floquet engineering of quantum materials, *Annual Review of Condensed Matter Physics* **10**, 387 (2019), <https://doi.org/10.1146/annurev-conmatphys-031218-013423>.

[28] A. Sen, D. Sen, and K. Sengupta, Analytic approaches to periodically driven closed quantum systems: methods and applications, *Journal of Physics: Condensed Matter* **33**, 443003 (2021).

[29] T. Kitagawa, E. Berg, M. Rudner, and E. Demler, Topological characterization of periodically driven quantum systems, *Phys. Rev. B* **82**, 235114 (2010).

[30] L. Jiang, T. Kitagawa, J. Alicea, A. R. Akhmerov, D. Pekker, G. Refael, J. I. Cirac, E. Demler, M. D. Lukin, and P. Zoller, Majorana fermions in equilibrium and in

driven cold-atom quantum wires, *Phys. Rev. Lett.* **106**, 220402 (2011).

[31] Z. Gu, H. A. Fertig, D. P. Arovas, and A. Auerbach, Floquet spectrum and transport through an irradiated graphene ribbon, *Phys. Rev. Lett.* **107**, 216601 (2011).

[32] M. Trif and Y. Tserkovnyak, Resonantly tunable majorana polariton in a microwave cavity, *Phys. Rev. Lett.* **109**, 257002 (2012).

[33] D. E. Liu, A. Levchenko, and H. U. Baranger, Floquet majorana fermions for topological qubits in superconducting devices and cold-atom systems, *Phys. Rev. Lett.* **111**, 047002 (2013).

[34] A. Kundu and B. Seradjeh, Transport signatures of floquet majorana fermions in driven topological superconductors, *Phys. Rev. Lett.* **111**, 136402 (2013).

[35] C. C. Wu, J. Sun, F. J. Huang, Y. D. Li, and W. M. Liu, Majorana fermions in a periodically driven semiconductor-superconductor heterostructure, *EPL (Europhysics Letters)* **104**, 27004 (2013).

[36] Q.-J. Tong, J.-H. An, J. Gong, H.-G. Luo, and C. H. Oh, Generating many majorana modes via periodic driving: A superconductor model, *Phys. Rev. B* **87**, 201109 (2013).

[37] A. A. Reynoso and D. Frustaglia, Unpaired floquet majorana fermions without magnetic fields, *Phys. Rev. B* **87**, 115420 (2013).

[38] N. H. Lindner, D. L. Bergman, G. Refael, and V. Galitski, Topological floquet spectrum in three dimensions via a two-photon resonance, *Phys. Rev. B* **87**, 235131 (2013).

[39] Y. T. Katan and D. Podolsky, Modulated floquet topological insulators, *Phys. Rev. Lett.* **110**, 016802 (2013).

[40] M. Thakurathi, K. Sengupta, and D. Sen, Majorana edge modes in the kitaev model, *Phys. Rev. B* **89**, 235434 (2014).

[41] J. K. Asbóth, B. Tarasinski, and P. Delplace, Chiral symmetry and bulk-boundary correspondence in periodically driven one-dimensional systems, *Phys. Rev. B* **90**, 125143 (2014).

[42] M. D. Reichl and E. J. Mueller, Floquet edge states with ultracold atoms, *Phys. Rev. A* **89**, 063628 (2014).

[43] P. M. Perez-Piskunow, L. E. F. Foa Torres, and G. Usaj, Hierarchy of floquet gaps and edge states for driven honeycomb lattices, *Phys. Rev. A* **91**, 043625 (2015).

[44] A. Agarwala, U. Bhattacharya, A. Dutta, and D. Sen, Effects of periodic kicking on dispersion and wave packet dynamics in graphene, *Phys. Rev. B* **93**, 174301 (2016).

[45] R. Roy and F. Harper, Abelian floquet symmetry-protected topological phases in one dimension, *Phys. Rev. B* **94**, 125105 (2016).

[46] S. Yao, Z. Yan, and Z. Wang, Topological invariants of floquet systems: General formulation, special properties, and floquet topological defects, *Phys. Rev. B* **96**, 195303 (2017).

[47] M. Thakurathi, D. Loss, and J. Klinovaja, Floquet majorana fermions and parafermions in driven rashba nanowires, *Phys. Rev. B* **95**, 155407 (2017).

[48] M. Rodriguez-Vega and B. Seradjeh, Universal fluctuations of floquet topological invariants at low frequencies, *Phys. Rev. Lett.* **121**, 036402 (2018).

[49] T. Čadež, R. Mondaini, and P. D. Sacramento, Edge and bulk localization of floquet topological superconductors, *Phys. Rev. B* **99**, 014301 (2019).

[50] U. Bhattacharya, S. Maity, A. Dutta, and D. Sen, Critical phase boundaries of static and periodically kicked long-range kitaev chain, *Journal of Physics: Condensed Matter* **31**, 174003 (2019).

[51] G. Floquet, Sur les équations différentielles linéaires à coefficients périodiques, *Annales scientifiques de l'École Normale Supérieure 2e série*, **12**, 47 (1883).

[52] M. McGinley and N. R. Cooper, Topology of one-dimensional quantum systems out of equilibrium, *Phys. Rev. Lett.* **121**, 090401 (2018).

[53] S. Bandyopadhyay, U. Bhattacharya, and A. Dutta, Temporal variation in the winding number due to dynamical symmetry breaking and associated transport in a driven su-schrieffer-heeger chain, *Phys. Rev. B* **100**, 054305 (2019).

[54] S. Bandyopadhyay and A. Dutta, Dynamical preparation of a topological state and out-of-equilibrium bulk-boundary correspondence in a su-schrieffer-heeger chain under periodic driving, *Phys. Rev. B* **100**, 144302 (2019).

[55] P. Fromholz, G. Magnifico, V. Vitale, T. Mendes-Santos, and M. Dalmonte, Entanglement topological invariants for one-dimensional topological superconductors, *Phys. Rev. B* **101**, 085136 (2020).

[56] T. Micallo, V. Vitale, M. Dalmonte, and P. Fromholz, Topological entanglement properties of disconnected partitions in the Su-Schrieffer-Heeger model, *SciPost Phys. Core* **3**, 12 (2020).

[57] S. Mondal, S. Bandyopadhyay, S. Bhattacharjee, and A. Dutta, Detecting topological phase transitions through entanglement between disconnected partitions in a kitaev chain with long-range interactions, *Phys. Rev. B* **105**, 085106 (2022).

[58] I. Peschel, Calculation of reduced density matrices from correlation functions, *Journal of Physics A: Mathematical and General* **36**, L205 (2003).

[59] G. Vidal, J. I. Latorre, E. Rico, and A. Kitaev, Entanglement in quantum critical phenomena, *Phys. Rev. Lett.* **90**, 227902 (2003).

[60] P. Calabrese and J. Cardy, Entanglement entropy and quantum field theory, *Journal of Statistical Mechanics: Theory and Experiment* **2004**, P06002 (2004).

[61] J. I. Latorre and A. Riera, A short review on entanglement in quantum spin systems, *Journal of Physics A: Mathematical and Theoretical* **42**, 504002 (2009).

[62] P. Calabrese and J. Cardy, Entanglement entropy and conformal field theory, *Journal of Physics A: Mathematical and Theoretical* **42**, 504005 (2009).